Coupled arc and droplet model of GMAW

T. P. Quinn*[1], M. Szanto[2], I. Gilad[2] and I. Shai[2]

A model of gas metal arc welding was developed that solves the magnetohydrodynamic equations for the flow and temperature fields of the molten electrode and plasma simultaneously, to form a fully coupled model. A commercial finite-element code was extended to include the effects of radiation, Lorentz forces, Joule heating and thermo-electric effects. The model predicts the shape of the free surfaces of the molten metal as the droplets form, detach, and merge with the weld pool. It also predicts the flow, temperature, and electric field. Material properties and the welding parameters are the input variables in the model. The geometry of the numerical model was constructed to fit an experimental apparatus using an aluminium electrode and an argon shielding gas. Droplet frequency measurements were used to verify the model's predictions. For a typical arc, the temperature of the plasma can range up to 20 000 K, where there is more uncertainty in the thermophysical properties of the plasma, and the properties in this range are highly non-linear. For this range, the material properties of the model were adjusted to obtain a better fit between the numerical and the experimental results. The model and experimental results were comparable.

Keywords: GMAW, Finite element finite volume model, Magnetohydrodynamics, Droplet frequency, Material property approximation

Introduction

Over 150 million pounds of electrode are welded by gas metal arc welding (GMAW) each year in the United States[1] but in many ways, GMAW remains an art form. In GMAW, an arc is created between the continuously fed, consumable electrode (the anode) and the workpiece. The electrode is fed through a copper tube (the contact tube) at the end of a torch where a large current (100–600 A) is applied. The melted electrode forms droplets that are projected through the arc to act as filler metal in the weld. A shielding gas is directed around the electrode and weld pool. The designer of the weld must select the proper filler material and the process parameters – the electrode feedrate, the current or voltage, and the distance between the contact tube and the workpiece. The designer must ensure that the weld has the proper profile (reinforcement shape, depth of penetration, etc.) and is free of defects. Because of the large thermal excursions and phase transformation of the material in the weld joint, residual stresses and structural distortion result. They can be minimised by making the welds in a particular order and by proper selection of the process parameters. However, the process variables are usually determined through experience or extensive experiments.[2–4] Practical models of the process will reduce the costs of the experiments and ensure the quality of the welds.

Models of GMAW have concentrated on the weld pool,[5–7] the arc,[8] and the anode[9–13] (for a complete review, see Ref. 14). There is a need for coupled models of the entire system. When Choo *et al.* coupled the arc model with a calculation of the free surface of the weld pool in GTAW,[15] they found that the flow within the arc and weld pool was much different as a result of the deformation of the weld pool surface. Recently, two-dimensional models have appeared that couple the arc with the anode;[16–22] Haidar[17–20] performed the most comprehensive computation on mild steel electrodes. None of these has concentrated on welding of aluminium and most use unique numerical codes that are often difficult for others to use.

The objective of the research presented here was to develop a coupled model of an electrode and the surrounding plasma using a commercial finite-element program. The model will serve as a part of the overall coupled electrode–plasma–weld pool model. Specifically, the model was developed for an aluminium electrode with an argon plasma. However, the model can be extended to other materials as well. In the present computation, the authors have focused on the droplet formation, its frequency, and its influence on the plasma after detachment and travel toward the weld pool.

Measurements and computational results indicate that at the hottest spots in the plasma, the temperature usually exceeds 20 000 K.[14,16,18] At that temperature, the material property data are uncertain. In addition, the temperature dependence of some properties is highly non-linear. This non-linearity increases the numerical effort, forcing very small time steps, and causing numerical difficulties in the convergence of the solution. Consequently, modified material properties were used so that the experimental results would compare with the model. The modified material properties also account for the physics that was not considered in the model such as heat of evaporation.

[1]Materials Reliability Division, National Institute of Standards and Technology, Boulder, CO 80305, USA
[2]Department of Mechanical Engineering, Ben-Gurion University, Beer-Sheva, Israel 84105

*Corresponding author, email quinn@boulder.nist.gov

Published by Maney on behalf of the Institute
Received 27 August 2003; accepted 8 January 2004
DOI 10.1179/174329305X29492

The principal result of the present work is the ability to predict the frequency of the metal transferred from the electrode, an important energy source for the welding pool in GMAW.

Model

There are three phases present in the system: (i) the solid of the electrode and workpiece, (ii) the liquid of the droplets, weld pool, and melt at the end of the electrode, and (iii) the plasma of the arc. The plasma was modelled as a single, magnetohydrodynamic fluid in local thermodynamic equilibrium. In the anode fall and cathode fall regions, special interface conditions were used to accommodate the heat transfer in these non-thermodynamic equilibrium regions.

The governing equations are as follows:

Conservation of momentum

$$\rho\left(\frac{\partial u_{\mathrm{i}}}{\partial t}+u_{\mathrm{j}}u_{\mathrm{i,j}}\right)=\sigma_{\mathrm{ij,j}}+\rho f_{\mathrm{i}} \tag{1}$$

where u is the velocity, ρ is the density, and t is time. The stress σ and body force f are given by

$$\sigma_{\mathrm{ij}}=-p\delta_{\mathrm{ij}}+\mu(u_{\mathrm{i,j}}+u_{\mathrm{j,i}})-{}^{2}\!/_{3}\mu\, u_{\mathrm{k,k}}\delta_{\mathrm{ij}} \tag{2}$$

$$f_{\mathrm{i}}=g_{\mathrm{i}}+\varepsilon_{\mathrm{ijk}}\, j_{\mathrm{j}}B_{\mathrm{k}} \tag{3}$$

where p is pressure, μ is viscosity, g is gravity, j is the current density and B is the magnetic field. The model considers all flow to be laminar.

Conservation of mass

$$u_{\mathrm{j,j}}=0 \tag{4}$$

Conservation of energy

$$\rho c_{\mathrm{p}}\left(\frac{\partial T}{\partial t}+u_{\mathrm{i}}T_{\mathrm{i}}\right)=(kT_{\mathrm{i}})_{\mathrm{i}}-pu_{\mathrm{i,i}}+\frac{j_{\mathrm{i}}\,j_{\mathrm{i}}}{s}-S_{\mathrm{R}} + \frac{5}{2}\,\frac{k_{\mathrm{b}}}{e}(T_{\mathrm{i}}\,j_{\mathrm{i}}) \tag{5}$$

where c_{p} is the specific heat, T is temperature, k is the thermal conductivity, k_{b} is the Boltzmann constant, e is the electron charge, and S_{R} is the radiant heat loss. The last term in the equation is the thermoelectric (Thompson) effect. Here it is assumed that the plasma is optically thin – the radiant energy lost from one part of the plasma is not absorbed by some other part of the plasma. The thermophysical properties μ, c_{p} and k are allowed to vary with temperature. The density ρ is held constant with temperature.

Maxwell's equations

$$B_{\mathrm{i,i}}=0 \tag{6}$$

$$e_{\mathrm{ijk}}B_{\mathrm{k,j}}=\varepsilon\,\frac{\partial \phi_{,\mathrm{i}}}{\partial t}+\mu_0\, j_{\mathrm{i}} \tag{7}$$

$$e_{\mathrm{ijk}}\phi_{,\mathrm{kj}}=-\frac{\partial B_{\mathrm{i}}}{\partial t} \tag{8}$$

where μ_0 is the permeability of free space, ε is the dielectric permittivity of free space, and ϕ is the electric potential. If arc initiation is not being studied, the dynamics of the electromagnetics are relatively unimportant, and the transient terms in equations (6)–(8) can be neglected, as was done in Refs. 17–19. This gives

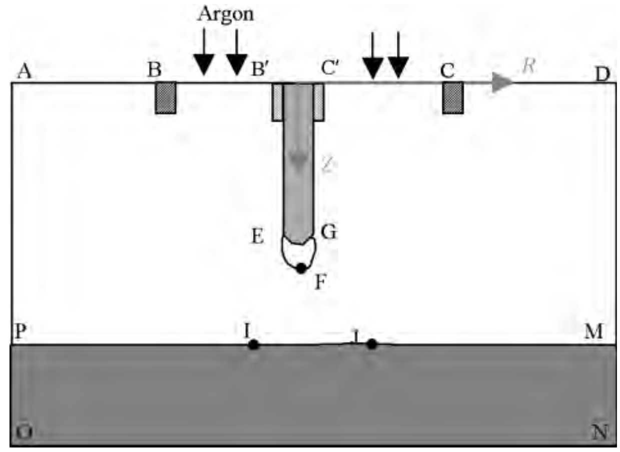

1 Simplified geometry of GMAW system used for describing boundary conditions

$$j_{\mathrm{i,i}}=0 \tag{9}$$

$$e_{\mathrm{ijk}}B_{\mathrm{k,\,j}}=\mu_0\, j_{\mathrm{i}} \tag{10}$$

$$j_{\mathrm{j}}=-s\phi_{,\mathrm{j}} \tag{11}$$

where s is the electrical conductivity. In equation (11) (Ohm's law), the terms $e_{\mathrm{ijk}}u_{\mathrm{j}}B_{\mathrm{k}}$ will be neglected as small compared to $s\phi_{\mathrm{j}}$, as was done in Refs. 17–20, 23.

Equations (1)–(5) and equations (9)–(11) form a complete set of 21 equations with 21 unknowns. Although implicitly written above in rectilinear coordinates, the equations have been solved in cylindrical coordinates. To reduce the computational effort, the model is axisymmetric which implies no translation of the torch relative to the workpiece. This model therefore corresponds to GMAW spot welding.

For the axisymmetric model, the self induced magnetic field B_θ is

$$B_\theta=\frac{\mu_0}{r}\int_0^{r} j_{\mathrm{r}}r\,\mathrm{d}r \tag{12}$$

The boundary conditions on the system are straightforward; the interface conditions are more complex. The inflow velocity of the shielding gas on boundaries B–B′ and C–C′ (Fig. 1), through the gas cup, was matched to the volumetric gas inflow rate. The velocity profile across B–B′ (C–C′) was taken as parabolic; the temperature of the incoming gas was set to T_0. For $0<r<r_0$

$$\Phi=V$$

$$u_{\mathrm{i}}=(0,0,v_{\mathrm{z}})$$

$$T=T_0 \tag{13}$$

where V is the potential from the power source, r_0 is the electrode radius, v_{z} is the electrode feed speed or, more commonly, the wire feed speed (WFS), and the triple corresponds to components of u in the r, θ, z directions. M–N–O–P is the workpiece and will be modelled as

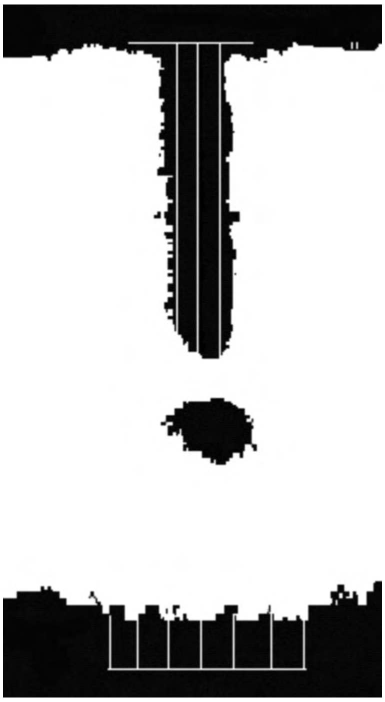

2 Binary image used to calculate droplet frequency

having $T=T_0$, and no velocity. The region I–J (30 mm diameter here) is modelled as having a zero potential, effectively making it the cathode spot. For comparison, the model was also run with M–N–O–P as having zero potential.

The interface conditions have been formulated following the lead of Jönsson *et al.*[8] The assumption that the plasma is in local thermodynamic equilibrium does not hold in the anode fall region and the cathode fall region. Two special interface conditions were used to accommodate these regions. Where the $j>0$ on B′–E–F–G–C′, a heat-generation term accounting for the thermoelectric effect and radiation was added to the anode (and subtracted from the plasma) of the form

$$q_a = \frac{5}{2}\frac{k_b}{e}(\hat{T}_a j_i j_i) - S_{net} \tag{14}$$

where $\hat{T}_a$ is the jump in temperature between the surface of the anode and the plasma some small distance (<0·05 mm, Ref. 16) away. S_{net} is the net radiant energy lost. Here, the conductive and convective heat transfer of the plasma on the anode surface will be calculated using the thermophysical properties of the plasma modelled as a single fluid as was done in Refs. 17–20. The sheath effects were ignored. The electrode was

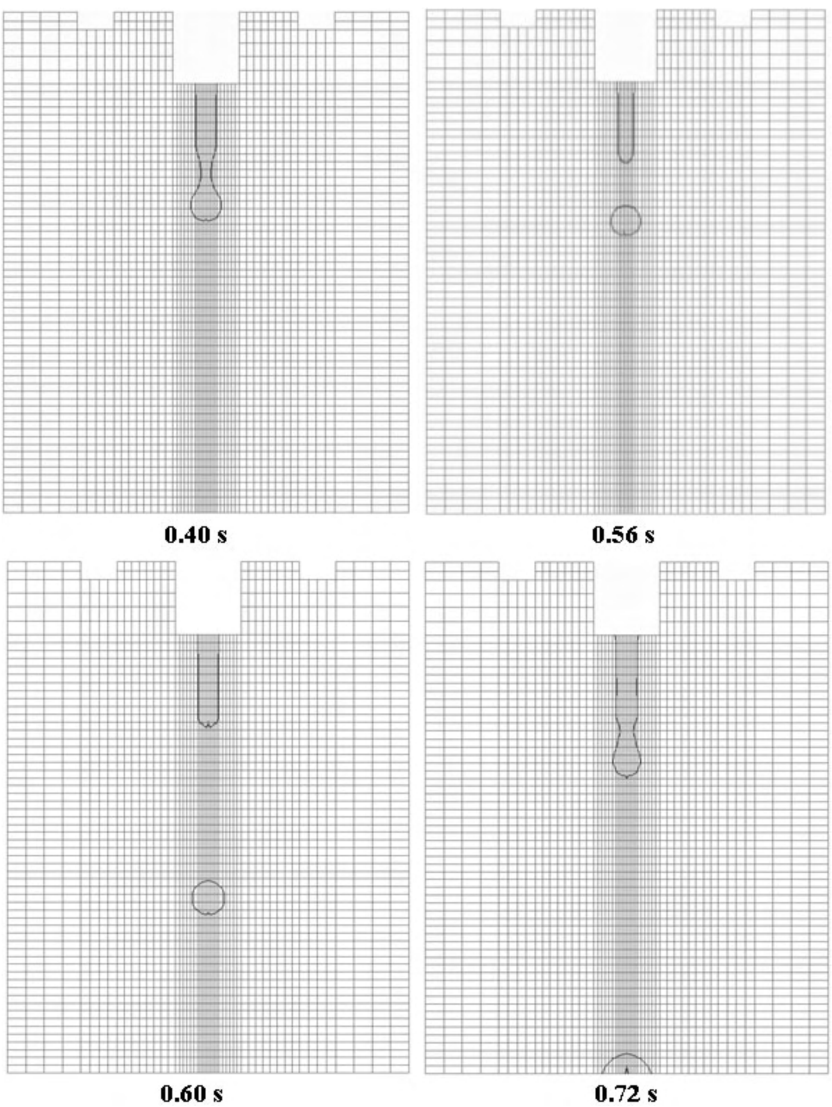

3 Droplet development and detachment in simplified model

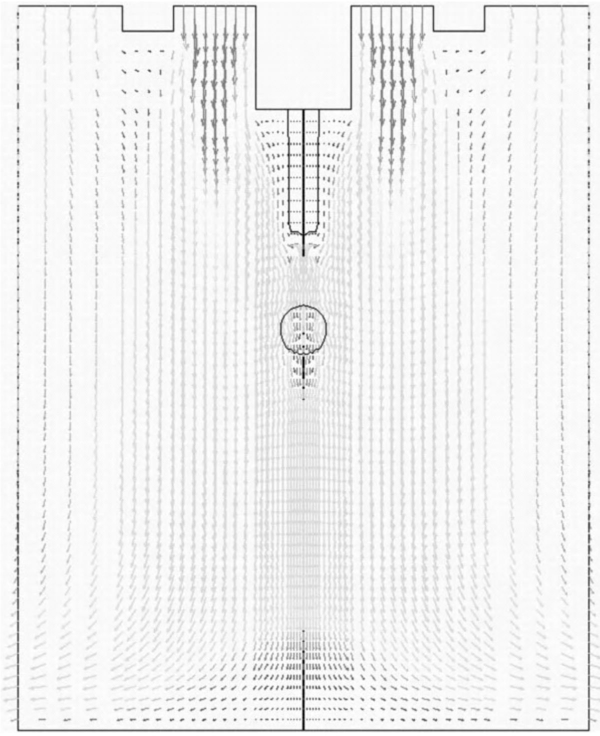

4 Velocity vector plot for simplified model

modelled as a blackbody emitter and the radiation impinging on the electrode from the plasma was neglected. A similar expression was used for the cathode spot (I–J in Fig. 1).

The mass flux from the surface of the molten metal owing to vaporisation was neglected (this can be partly accounted for by adjusting the thermophysical properties of the plasma). The pressure p_γ on the surface of the liquid metal because of surface tension was modelled as

$$p_\gamma = \gamma\left(\frac{1}{R_1} + \frac{1}{R_2}\right) \tag{15}$$

where γ is the coefficient of surface tension, and R_1 and R_2 are the principal radii of curvature of the surface. Surface tension is modelled as constant and not a function of temperature.

The equations were solved numerically, using a hybrid finite-element and finite-volume technique. A commercial CFD code[24] was extended with self-coded subroutines that account for special effects such as self-induced magnetic field, or radiation. The Navier–Stokes equations were solved using the Galerkin finite element method.

A Eulerian approach is used where the mesh is fixed as in Ref. 16. The materials, the plasma and metal, flow through the mesh. Each cell is filled either with a single material or with a mixture of both materials.

The fluid volume is represented by the characteristic marker concentration F which moves with the fluid. The value of F is unity within the tracked, first fluid (molten metal) and zero within the second fluid (plasma). A step gradient in F marks the surface between the two materials. The time dependence of F is governed by

$$\frac{\partial F}{\partial t} + \mathrm{u}\cdot\nabla F = 0 \tag{16}$$

A sharp gradient in F exists in elements that contain both materials. The marker concentration is discretised

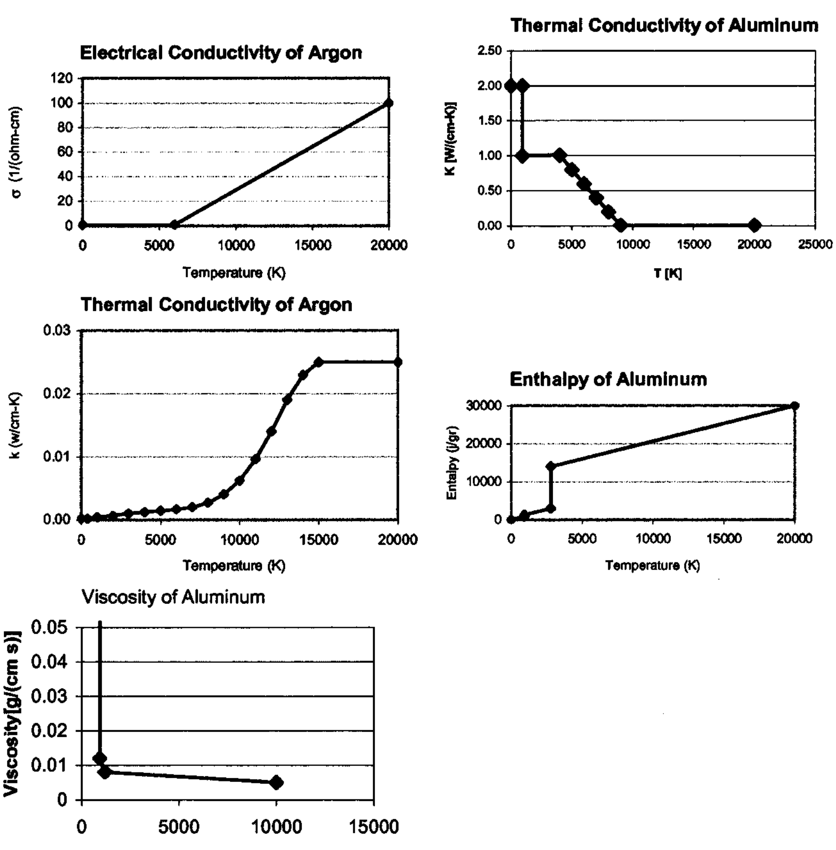

5 Temperature-dependent material properties used in the present work

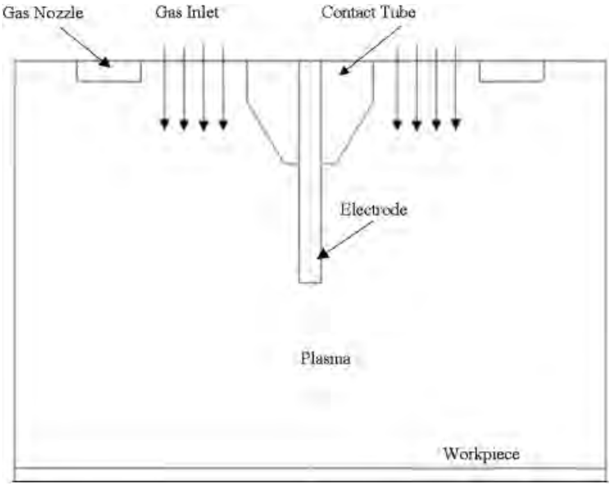

6 Geometry of experimental torch

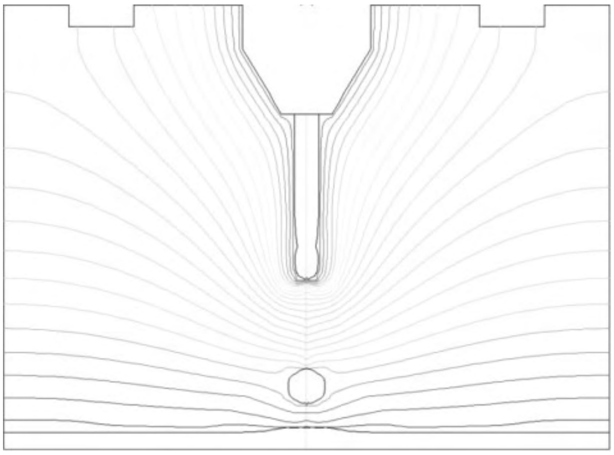

8 Equipotentials; electric potential at electrode is 22·3 V, and at workpiece, under the drop, it is 0 V

by

$$f_i = \frac{1}{V_i}\int F\,\mathrm{d}V_i, \text{ for element } i \tag{17}$$

where V_i is the volume of element i and f_i refers to the fractional fill state. For an element filled fully with the first material $f_i=0$, and with the second material $f_i=1$. For an element with partial fill of the materials, $0<f_i<1$.

Each material property P_i, of an element i has the value of

$$P_i = P_a f_i + P_b(1-f_i) \tag{18}$$

where P_a and P_b are, respectively, the properties of material 'a' and 'b'. The large differences in material properties between the plasma and the metal can cause an element that has a very small f_i to have an inaccurate material property because of the orders of magnitude differences between P_a and P_b. Therefore, the mesh near the interface needs to be relatively dense to allow for convergence.

The location of the interface between the plasma and the molten metal/solid is required in order to apply the interface conditions. The location is found by evaluating the fill state of the element and the fill state of its neighbouring elements (the gradient of the fill state). However, the computation of the orientation of the interface inside the element is not accurate. This is a source of an error that propagates throughout the computation, especially because a typical analysis consists of a large number of small time steps. A dense mesh minimises such errors but increases the computational effort (time and memory).

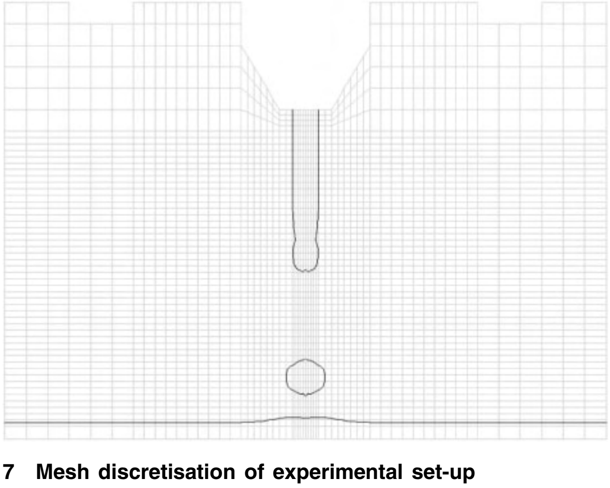

7 Mesh discretisation of experimental set-up

An alternative approach is a Lagrangian mesh that deforms with the boundary. In such an approach, the interface is well defined, but because of the large distortion of elements, a continuous re-meshing needs to be performed. In addition, because of the distortion of the mesh, the computation of the magnetic field (equation (12)) is complicated.

Experimental verification

The experiments were conducted as in Ref. 9. Bead-on-plate welds were made with a 1·19 mm ER-1100 electrode (>99% pure Al). A low-noise regulator was used as described in Ref. 25 to maintain constant current. To obtain measurements of the electrode extension, arc length, and droplet frequencies, a 10 mW He–Ne laser and 632 nm bandpass filter were used to create a shadowgraph of the electrode and base plate.[26] The shadowgraph images were recorded on a high-speed video system. The contact tube, the electrode, and the workpiece were imaged. The images were processed digitally to extract the electrode extension and the contact tube-to-work distance as a function of time. By choosing an appropriate threshold value, a binary image is created (Fig. 2). A baseline is set at the end of the contact tube and the distance to the end of the droplet is measured with three video lines. The average of the three is taken as the distance from the end of the contact tube to the end of the droplet. The resulting time sequence can be analysed with a power-spectrum density calculation to find the droplet frequency.

The current was measured with a Hall-effect transducer with an absolute error of 1%. The voltage between the torch and the baseplate was measured within 0·5% absolute error. The axial velocity of the electrode or feed speed v_z was measured as the electrode entered the wire feeder: a pinch roller (16 mm dia.) was attached to an optical encoder (5000 pulses rev.$^{-1}$) and the resulting pulse train was frequency converted to give a voltage signal proportional to v_z. The r.m.s. uncertainty from calibration tests for the transducer was 2 mm s^{-1}. The contact tube-to-work distance was set at 17 mm.

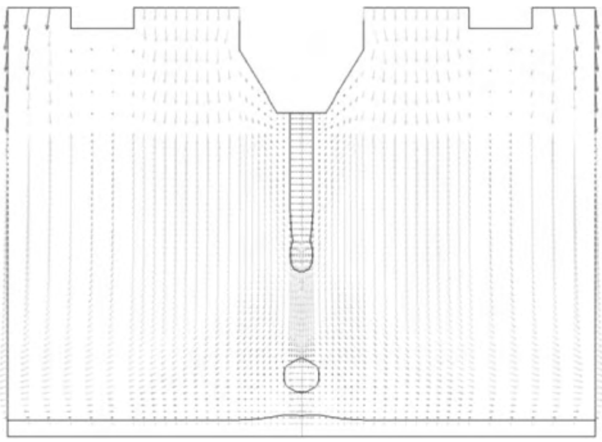

9 Velocity vectors

Computational results and discussion

Preliminary computations using a simplified geometry of the torch, following Fig. 1, were used to identify the important parameters in the model and identify the numerical methods necessary for efficient numerical convergence. After the preliminary computations, the geometry of the model was fitted to the torch of the experimental apparatus.

The preliminary mesh as a droplet develops and detaches in it is presented in Fig. 3. In order to accurately calculate the droplet shape, the mesh size at the electrode tip and at the adjacent elements of the argon is set to 0·1 mm. To minimise numerical errors, the maximum time step is set to 5×10^{-6} s; similar orders of magnitude were chosen by Haidar[17] (cell sizes of 0·075 mm and time steps of 25×10^{-6} s). Here, an aluminium electrode and workpiece were used with argon as the shielding gas. In the simplified model, the anode has a diameter 1·2 mm, with feedrate of 100 mm s^{-1}. The average inflow shielding gas velocity was 5000 mm s^{-1}. The overall voltage difference, between the electrode and the workpiece, was set to 20·3 V. A complete drop development and detachment is presented in Fig. 3. The current interacting with the induced magnetic field causes a body force (the 'pinch' force[27]) that is pointed toward the centre of the plasma. The velocity and streamline plot in Fig. 4 demonstrates the result of this force on the flow of the shielding gas.

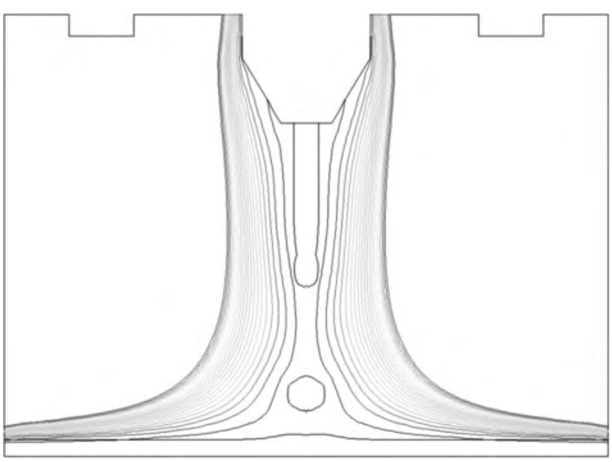

10 Streamline plot at arc area

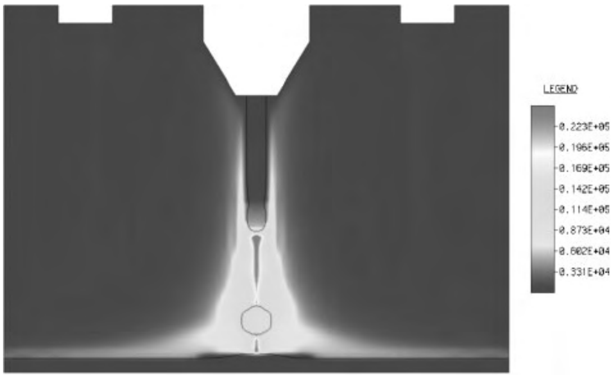

11 Temperature distribution; temperature is in K

A typical computational time for the preliminary mesh on a 1 GHz, PC-based workstation was 30 h to simulate the first drop until its detachment (Haidar[17] reported 20 h on a supercomputer).

The temperature range in the plasma, from ambient to over 15 000 K, resulted in high non-linearity of the material properties. For example, the electrical conductivity of the argon has an almost exponential dependence on temperature,[27] and both the magnetic field and the Joule heat depend on its value. This high non-linearity increases the numerical effort by requiring small time steps which can cause numerical difficulties in the convergence of the solution. Moreover, at high temperatures, there is uncertainty in the available property data. To account for the differences in properties of the actual shielding gas (it may include aluminium vapour), to decrease computational effort, and to account for some physical effects that are not included in the model, such as heat of evaporation, compensated material properties were introduced. The compensated properties were found so that the model fits the experimental results while reducing the computational effort. This approach is one of the significant contributions of the current work, since in a relatively simple way the computational model can be calibrated by experiments.

Note that in the VOF method (used here as well as in Refs. 16–20, 28), only a slight variation in the density is allowed. Physically, this is an adequate model for the aluminium, but in the plasma, the density variation is high. Therefore, special care was taken when selecting a constant value for the density of the plasma by matching the overall results of the model to the experimental measurements.

Properties that were taken as constant are listed in Table 1, whereas those that were assumed dependent on temperature are shown in Fig. 5.

Once the thermophysical property curves/constants were identified with the simplified geometry, the actual

Table 1 Constant material properties used in the present work

Property	Unit	Aluminium	Argon
Surface tension	N cm^{-1}	0·009	–
Density	g cm^{-3}	2·7	0·0008
Dynamic viscosity	g cm^{-1} s^{-1}	–	0·0025
Specific heat	J g^{-1} K^{-1}	–	50
Magnetic permeability	H cm^{-1}	–	0·00012
Electrical conductivity	$(\Omega$ cm$)^{-1}$	250 000	–

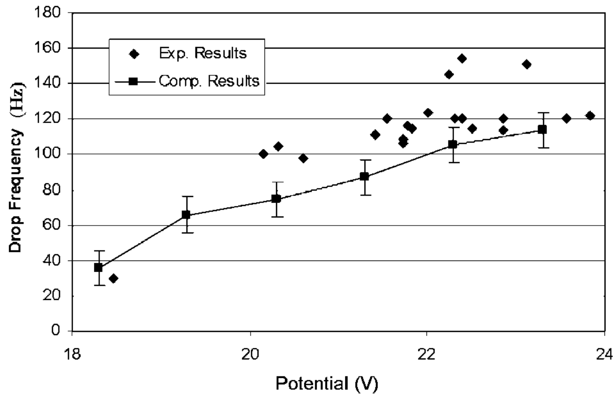

12 Experimental and computational results of drop frequency as a function of voltage difference; error bars on computational results are standard deviation of drop frequency calculated between individual droplets

geometry of the experimental apparatus was used (Fig. 6). The mesh again was denser in the region where droplets form and travel. Mesh discretisation with representative plots of the drop propagation through the mesh is presented in Fig. 7. The droplet frequency was used to test the sensitivity of the model using the preliminary mesh to changes in the assumptions of the boundary conditions and parameters. In order to calibrate the exact model to the experimental results, characteristic experiments with a potential difference of 22·3 V and wire feedrate of 94 mm s^{-1} were performed. The average inflow shielding gas velocity was 1800 mm s^{-1}. To stay away from the initial transient effects, the computation concluded after more than 10 drops. The frequency of the droplet was measured experimentally to be between 100 and 120 Hz. The droplet frequency for the model results was calculated using the time difference between two consecutive drop detachments. The minimum and maximum frequencies were 95 and 115 Hz, respectively, whereas the average was 105 Hz. Those computational results agree well with the experiments. Note that the model predicts that the time between drops varies and is not constant which is also observed in experiments.

Typical electric field, velocity vector, streamline, and temperature plots in the actual experimental model are presented in Fig. 8 through Fig. 11, respectively. Note that because of the model limitation that there is no vaporisation of the molten metal, the model probably overpredicts the temperature of the droplets in Fig. 11 at about 10^4 K.

To verify the model predictions, droplet frequency predictions (using the above identified material properties) were made from 18 to 24 V (Fig. 12). Linearly interpolating the computational data, the r.m.s. difference between it and the experimental data is 23 Hz. Remember that the material data are optimised using only one data point and the resulting predictions of the droplet frequency are comparable (Fig. 12).

Summary

A numerical model of the electrode–plasma was developed for aluminium. The model is based on a commercial CFD code augmented with self-coded subroutines. For a typical arc, the temperature of the plasma can range up to 20 000 K where there is more uncertainty in the thermophysical properties of the plasma, and the properties in this range are highly non-linear. For this range, the material properties of the model were adjusted to obtain a better fit between the numerical and the experimental results using only a single data point. The model and experimental results were comparable from 18 to 24 V. This approach is one of the significant contributions of the present work, since in a relatively simple way the computational model can be calibrated by experiments. Once the model and the compensated values were established, the computation simulates the process and is ready for different working parameters.

References

1. U. S. Census: 'Welding and soldering equipment manufacturing'; 1997, United States Department of Commerce.
2. I. A. Mcconnell and N. A. Mcpherson: *Weld. J.,* 1997, **76**, 412s–416s.
3. J. C. Mcglone, J. Doherty and S. B. Jones: Proc. Welding Fabrication in the Nuclear Industry, British Nuclear Energy Society, 1979, 283–289.
4. M. Galopin and E. Boridy: *Soudage Techniques Connexes*, 1983, **37**, 403–412.
5. T. Zacharia, A. H. Eraslan and D. K. Aidun: *Weld. J.,* 1988, **67**, 18s–27s.
6. P. Tekriwal and J. Mazumder: *Weld. J.,* 1988, **67**, 150s–156s.
7. J.-W. Kim and S.-J. Na: *Weld. Joining Proc.,* 1991, 51, 159–173.
8. P. G. Jönsson, J. Szekeley, R. B. Madigan and T. P. Quinn: *Weld. J.,* 1995, **74**, 93s–102s.
9. T. P. Quinn, R. B. Madigan and T. A. Siewert: *Weld. J.,* 1994, **73**, 241s–248s.
10. Y.-S. Kim, D. M. McEligot and T. W. Eager: *Weld. J.,* 1991, **70**, 20s–31s.
11. J. H. Waszink and G. J. van den Heuvel: Proc. Int. Conf. on 'Arc physics and weld pool behavior', The Welding Institute, 1979, 227–239.
12. S. K. Choi, S. H. Ko, C. D. Yoo and Y.-S. Kim: *Weld. J.,* 1998, **77**, 45s–51s.
13. S. K. Choi, C. D. Yoo and Y.-S. Kim: *Weld. J.,* 1998, **77**, 38s–44s.
14. P. G. Jönsson, J. Szekeley, R. T. C. Choo and T. P. Quinn: *Model. Simul. Mater. Sci. Eng.,* 1994, **2**, 995–1016.
15. R. T. C. Choo, J. Szekely and R. C. Westhoff: *Weld. J.,* 1990, **69**, 346s–361s.
16. J. Haidar and J. J. Lowke: *J. Phys. D Appl. Phys.,* 1996, **29**, 2951–2960.
17. J. Haidar: *J. Appl. Phys.,* 1998, **84**, 3518–3529.
18. J. Haidar: *J. Appl. Phys.,* 1998, **84**, 3530–3540.
19. J. Haidar: *J. Phys. D Appl. Phys.,* 1998, **31**, 1233–1244.
20. J. Haidar: *J. Appl. Phys.,* 1999, **85**, 3448–3459.
21. S. W. Simson and P. Zhu: *J. Phys. D Appl. Phys.,* 1995, **28**, 1594–1600.
22. H. G. Fan and R. Kovecevic: *Metall. Mater. Trans. B*, 1999, **30B**, 791–801.
23. C.-H. F. Liu: 'Numerical analysis of the anode region of high intensity arcs'; 1977, Minneapolis, The University of Minnesota.
24. Fluid Dynamics International: 'Theory, user manuals'; 1998, Fluid Dynamics International.
25. P. R. Heald, R. B. Madigan, T. A. Siewert and S. Liu: 'Droplet transfer modes for a MIL 100S-1 GMAW electrode'; 1991, Report No. NISTIR 3976, Gaithersburg, MD, NIST.
26. C. D. Allemand, R. Schoeder, D. E. Ries and T. W. Eager: *Weld. J.,* 1985, **64**, 45–47.
27. J. F. Lancaster: in 'The physics of welding'; 1986, (ed. J. F. Lancaster), Oxford, Pergamon Press.
28. J. Haidar: *J. Phys. D Appl. Phys.,* 1999, **32**, 263–272.